Journal of Aerosol Science 57 (2013) 114–124

Contents lists available at SciVerse ScienceDirect

Journal of Aerosol Science

journal homepage: www.elsevier.com/locate/jaerosci

On pinchoff behavior of electrified droplets

Min Wook Lee, Na Young Kim, Sam S. Yoon *

School of Mechanical Engineering, Korea University, Seoul 136-713, Republic of Korea

ARTICLE INFO

Article history:
Received 26 January 2012
Received in revised form
17 September 2012
Accepted 19 September 2012
Available online 28 September 2012

Keywords:
EHD (electrohydrodynamics)
Microdripping
Pinchoff
Electrical conductivity
Topology
Aspect ratio

ABSTRACT

Electrohydrodynamic (EHD) inkjets produce micro- and nano-sized droplets by using an electrostatic field imposed between the nozzle and the substrate. The conducting droplet about to separate (or "pinchoff") from the continuous fluid undergoes a transitional topological change under the competition between the electrical force due the imposed electrostatic field and the forces arising from liquid's own thermo-physical properties, such as viscosity and surface tension. This study is the first attempt to elucidate the pinchoff topology and characteristics of an electrified liquid droplet experimentally. Aspect ratio, which is defined as the ratio of the vertical (b) to horizontal (a) dimensions of a pinchoff droplet, is reported. The range of the dimensionless charging level (N_e) that yields stable microdripping droplets is also reported for various liquids (i.e., acetone, methanol, ethanol, water, dimethylformamide, and methoxyethanol). We experimentally showed that pinchoff topology is a function of both the charge level (N_e) and the electrical conductivity (K) of the droplet liquid. Despite the different properties of the liquids examined, pinchoff topologies were similar when N_e and K were set as constants.

1. Introduction

Electrohydrodynamic (EHD) inkjets have received much attention because of their high-resolution printing using micro- and nano-sized droplets, which are produced when an electrostatic field is imposed between the nozzle and the substrate (Choi et al., 2008; Wu & Russel, 2009). Because EHD inkjets yield such small droplets, it is particularly well suited for printing electronics applications, including fabrication of conductive microtracks and microinterconnects (Eom et al., 2008, 2009; Wang et al., 2009a, 2009b; Wang & Stark, 2010). Also, because they carry out noncontact printing, they do not damage the substrate (Cheng et al., 2005). In addition to inkjet printing, EHD can be used for spray coating, agricultural spraying, separation processes, and mass spectrometry (Jaworek & Sobczyk, 2008; Miao & Xiao, 2002).

The idea of generating droplets or sprays in the presence of an electric field dates back to Gilbert (1628). Rayleigh (1882) determined the stability of an isolated, perfectly conducting charged droplet; this stability is often referred to as the Rayleigh limit. Taylor (1964) identified the conical angle of 49.3° as a specific self-similar solution – the celebrated "Taylor cone." Yarin et al. (2001) demonstrated a non-self-similar solution at the cone angle of 33.5°. Harris & Basaran (1993) numerically calculated a cone angle of slightly less than 40° using a boundary element method. Zhang & Basaran (1996) experimentally investigated the dynamics of liquid threads and the generation of satellite droplets in various electric fields. Notz & Basaran (1999) numerically simulated the high curvature of an inviscid, perfectly conducting droplet about to separate (or "pinchoff") from the continuous fluid using the Galerkin finite-element method. In a sequel numerical

* Corresponding author. Tel.: +82 2 3290 3376; fax: +82 2 926 9290.
E-mail address: skyoon@korea.ac.kr (S.S. Yoon).

0021-8502/$ - see front matter © 2012 Elsevier Ltd. All rights reserved.
http://dx.doi.org/10.1016/j.jaerosci.2012.09.003

simulation, Collins et al. (2007) solved the axisymmetric Navier–Stokes equation and thus included the viscous effect on the breakup time, the ratio of the sizes of the primary to satellite droplets formed at pinchoff, and their Coulombic stability. Collins et al. (2008) studied the effect of electrical conductivity on the pinchoff behavior by varying the dimensionless charge relaxation time, $\alpha=\tau_e/\tau_\sigma$, from 0.0237 to 2.37 at a fixed charging level ($N_e=15$) and Ohnesorge number ($Oh=0.1$). Surprisingly, there have been few experimental studies on the pinchoff topology and characteristics of an electrified droplet since Zhang & Basaran (1996). Table 1 compares the range of governing parameters (i.e., *We*, *Re*, *Ca*, *Oh*, N_e, τ_e, τ_f, τ_σ, and α) between the aforementioned studies and our current experimental work.

From the viewpoint of fluid dynamics, pinchoff behavior is of great interest because of the richness of the underlying physics. Pinchoff is a singularity event at a finite time. This singularity event, which includes recoiling and satellite droplet formation, influences the topology of the electrified droplet after the event. In general, pinchoff behavior can be categorized into four distinct regimes: If $Oh \ll \Theta(1)$, the *potential* or *inviscid* regime is presumed, where inertial and capillary forces compete. If $Oh \gg \Theta(1)$, the *viscous* regime is presumed where viscosity and capillary force compete for domination. If $Oh \approx \Theta(1)$, the *viscous-inertial* regime is presumed where inertial, viscous, and capillary forces all compete. Lastly, when approaching to pinchoff, the thread becomes sufficiently small such that the local Reynolds number approaches zero, in which case the relative viscous force becomes dominant; this phenomenon is known as the *Stokes* regime where $Oh \gg \Theta(1)$. The shear stress of the surrounding fluid or air is comparable to that of the liquid. As a result, both fluids show the *Stokes* flow characteristics (Basaran, 2002; Lister & Stone, 1998). In this *Stokes* regime, inertial force is negligible but the surface tension force and viscous force compete for domination.

To determine the specific regime, the capillary length (l_σ) and the viscous length (l_μ) of the droplet are compared to the characteristic length (l_{char}) of the droplet. The characteristic length can be as large as the nozzle diameter or as small as the diameter of the long slender filament (or thread) that connects the liquid and the pendant droplet; see Fig. 1 (Kang et al., 2011; Lee et al., 2012). The viscous length of water, for example, can be as small as a few tens of nanometers. Viscous

Table 1
Governing parameters of the previous studies and the current experimental work.

Literature review	$We \times 10^8$	$Re \times 10^2$	$Ca \times 10^7$	$Oh \times 10^3$	N_e	$\tau_e \times 10^8$	τ_f	τ_σ	$\alpha \times 10^5$
Zhang & Basaran (1996) **(EXP)**	298–0.24×10^8	33–6631	90.4–3.62×10^4	5–7	0–0.43	8×10^{-2}–170	10^{-6}	0.0074–0.0075	0.0108–22.7
Notz & Basaran (1999) **(NS)**	NA	NA	NA	NA	0–26	0	0.77	0.0075	0
Collins et al. (2007) **(NS)**	NA	NA	NA	1–10,000	0–7.5	NA	NA	NA	NA
Collins et al. (2008) **(NS)**	NA	NA	NA	100	15	NA	NA	NA	2.37×10^3–2.37×10^5
Present studies (EXP)	3.39–8.72	3.36–14.25	5.74–23.8	2.0–8.1	0–21.7	2.69–129	14.48	0.0019–0.003	1–68.4

Note that NS and EXP are abbreviation for Numerical Simulation and Experiment, respectively. The Weber, Reynolds, Capillary, and Ohnesorge numbers are defined as $We=\rho U^2 d/\sigma$, $Re=\rho U d/\mu$, $Ca=We/Re$, and $Oh=We^{0.5}/Re$, where ρ is density, $U=Q/(\pi R^2)$ is average velocity, d is the nozzle diameter (c.f., $d=2R$), and σ is surface tension. $N_e=\varepsilon_o V^2/(2R\sigma)$ is the dimensionless charging level, where ε_o, and V are the electric permittivity of free space and applied voltage at the nozzle, respectively. $\tau_e=\varepsilon/K$ is charge relaxation time in seceonds, where ε is the liquid permittivity and K is the electrical conductivity. $\tau_f=R/u$ is the fluid characteristics time in seceonds. $\tau_\sigma=(\rho R^3/\sigma)^{0.5}$ is the capillary time in seceonds. $\alpha=\tau_e/\tau_\sigma$ is the dimensionless charge relaxation time; the lower the α, the higher the conductivity.

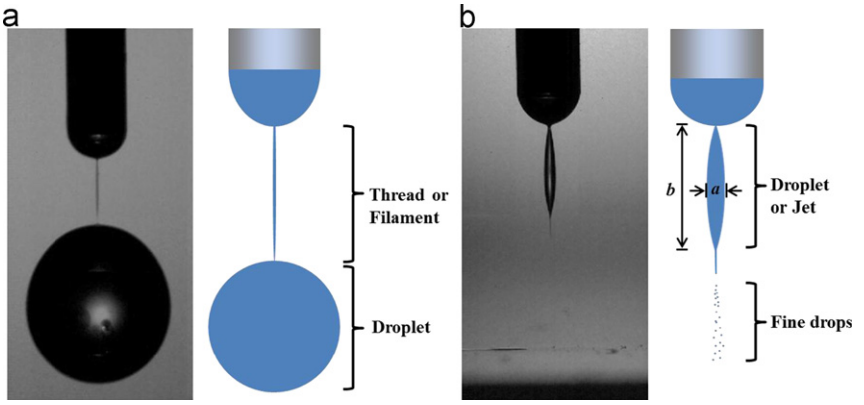

Fig. 1. Experimental (left) and schematic (right) images showing the distinction between (a) the gravitational dripping ($V_o=0$ kV) and (b) the EHD microdripping ($V_o=6.5$ kV).

forces can be neglected as long as the characteristic length is greater than the viscous length. While approaching the singularity event in which the filament diameter is comparable to the viscous length (i.e., a few tens of nanometer), viscosity plays an important role, as mentioned earlier. However, the analysis of the phenomenon at this brief time during which the filament diameter nears zero is beyond the scope of the current study as the experimental investigation of this singularity event is impossible even with the most advanced optical image diagnostics. This experimental limitation was the motivation behind the numerical investigation of Collins et al. (2008). In addition, gravitational effects are considered unimportant because the characteristic length is almost always much smaller than the capillary length (i.e., $l_{\text{char}} \ll l_{\sigma}$) in the microdripping regime, which is the main regime of the current study (Lee et al., 2012). All liquids used in this study have low viscosities, so their flows are considered nearly inviscid and capillary-dominant.

This report investigates the effects of electrical conductivity and surface tension of a droplet and the voltage level imposed between the nozzle and the substrate on the pinchoff behavior of the droplet. The viscosity effect of the liquid on the bulging of the pinchoff droplet is also investigated. As shown in Fig. 1(b), the electric charge elongates the pendant droplet. In extreme cases (high voltages), the ejected liquid forms an almost cylindrical jet connecting the nozzle and the substrate; no droplet is formed. This large-aspect-ratio cylindrical jet is subject to Rayleigh *jet* (not the Rayleigh *limit*) instabilities, whose linear and nonlinear effects yield a primary droplet and smaller satellite droplets, which form a nonuniform distribution of droplet sizes. From an academic perspective, the elongation, instability, and topology of a pinchoff droplet are of interest to fluid dynamicists; but from a practical perspective, information regarding the aspect ratio is of interest when setting the nozzle-to-substrate distance prior to printing (Jang et al., 2009; Nguyen et al., 2009). In general, the shorter this distance, the lower the power consumption. However, an unwanted high-voltage spark, "Coronal discharge," may occur when the nozzle-to-substrate distance is too small; this spark should be avoided (Yudistira et al., 2010).

2. Experimental setup

Fig. 2 is a schematic of the experimental setup of the EHD droplet-generation system. The primary competing forces are the surface tension; viscous, electrostatic forces; and gravitational forces. In the experiments, the viscous (e.g., $l_{\mu} \ll l_{\text{char}}$) and gravitational forces are not considered in the microdripping regime (e.g., $l_{\text{char}} \ll l_{\sigma}$); see Table 2. A Taylor cone is formed at the nozzle tip under the actions of surface tension and electrostatic stresses on the surface of the equipotential Taylor (1964) cone. A conical surface is formed during charge accumulation at the cone's apex. This phenomenon of charge accumulation leads to surface destabilization and eventually droplet ejection. The size of the droplet can be controlled by tuning the frequency of the applied voltage (Lee et al., 2012). The following parameters are related to droplet size and velocity: applied voltage (V), frequency (f), free space permittivity (ε_o), and fluid surface tension (σ) and viscosity (ν) (Choi et al., 2008; Jayasinghe & Edirisinghe, 2002; Yu et al., 2007).

Liquid is supplied to the stainless-steel nozzle (EFD, 18 gauge, inner and outer diameters of 0.84 and 1.27 mm, respectively) by a syringe pump (KDS 100). A multi-function synthesizer (NF Corporation, WF 1973) generates a step-function signal, which is sent to the HV-amplifier (TREK 10/40 A) for thousand-fold amplification. The amplified signal (voltage) is supplied to the conducting needle, which is directly connected to the syringe pump. A high-speed camera (Vision Research Inc., Phantom 7.3) with a zoom lens (1.56 μm/pixel) and Halogen lamp (250 W) captures magnified

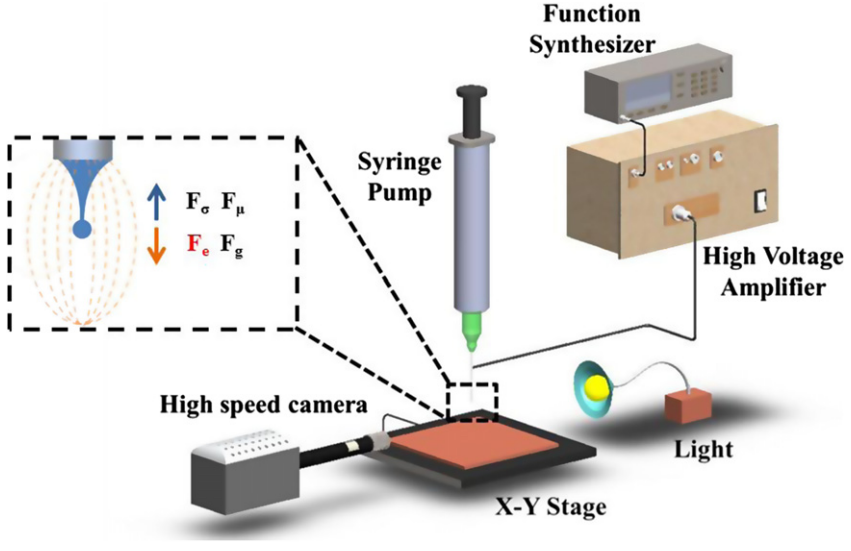

Fig. 2. Schematic of the experimental setup. Competing forces during the droplet pinchoff is also depicted. Note that F_σ is the surface tension force; F_μ is the viscous force; F_e is the electrical force; F_g is the gravitational force.

Table 2
Properties of the working liquids at 20 °C.

Working fluids	ρ [kg/m^3]	K [μS/cm]	$k=\varepsilon/\varepsilon_o$	μ [mPa s]	σ [mN/m]	$l_\sigma=(\sigma/\rho g)^{1/2}$ [10^3 m]	$l_\mu=\mu^2/(\rho\sigma)$ [10^8 m]
Acetone	793	0.2	21.1	0.31	23.7	1.75	0.51
Methanol	791	0.31	33.6	0.59	22.6	1.71	1.95
Ethanol	789	0.7	25.2	1.20	22.1	1.69	8.26
DI Water	1000	0.06	80.2	1.00	71.9	2.71	1.40
DMF	944	1.21	36.7	0.92	32.9	1.88	2.73
Methoxyethanol	930	0.08	16.9	1.54	30.8	1.84	8.28

Table 3
The dimensionless groups governing the flow physics for the solvents used in the current study.

Working fluids	$We\times10^8$	$Re\times10^2$	$Ca\times10^7$	$Oh\times10^3$	N_e	$\tau_e\times10^8$	τ_f	τ_σ	$\alpha\times10^5$
Acetone	8.17	14.25	5.74	2.0	12.4–21.7	9.35	14.48	0.0029	3.20
Methanol	8.55	7.47	11.4	3.9	11.7–18.1	9.75	14.48	0.0029	3.26
Ethanol	8.72	3.66	23.8	8.1	11.2–16.4	3.18	14.48	0.0030	1.05
DI Water	3.39	5.55	6.12	3.3	7.5–8.3	129	14.48	0.0019	68.4
DMF	7.01	5.72	12.3	4.6	10.7–21.2	2.69	14.48	0.0027	1
Methoxyethanol	7.38	3.36	21.9	8.1	10.3–13.7	18.7	14.48	0.0028	6.73

Note that τ_e, τ_f, τ_σ are given in seconds, while all other parameters are dimensionless.

images of ejected ink droplets. Snapshots are taken at 100-μs intervals. The distance between the nozzle tip and the well-polished copper substrate is fixed at 5 mm. One aspect ratio measurement is the average value of measurements taken in 10–15 repeated tests. All measurements of pulse duration and applied voltage have errors $<5\%$ based on repeated tests. The working fluids are acetone, methanol, ethanol, DI water, dimethylformamide (DMF), and methoxyethanol, whose thermo-physical properties are summarized in Table 2. The viscosity and surface tension of the working fluid are measured with a viscometer (LVDV-I+CP, Brookfield) and a surface-tension meter (DST 60A, Surface & Electro-Optics Co,. Ltd) at room temperature. All measurements are repeated three times, and the average is reported. The volumetric flow rate is fixed at 0.2 ml/h in all cases. The dimensionless groups governing the flow physics for the solvents used are summarized in Table 3.

3. Results and discussion

Fig. 3 shows the effect of the dimensionless charging level (N_e) on the pinchoff behavior at various electrical conductivities (K) for water and DMF. The results are obtained at the instant the droplet is about to detach from the nozzle, the so called "pinchoff" instant. The charge level is defined as $N_e=\varepsilon_o V^2/(2R\sigma)$, where ε_o, V, R, and σ are the electric permittivity of free space, applied voltage at the nozzle, capillary radius (i.e., nozzle radius), and surface tension of the liquid, respectively. The gravitational bond number, Bo, represents the competition between the gravitational and capillary forces and is calculated by $Bo=gR^2\rho/\sigma$. Bo shows a small variation in the cases shown in Fig. 3 and, thus, its effect on the pinchoff behavior can be considered negligible. It should be pointed out that perfect microdripping does not occur for every type of fluid and occurs primarily when the droplet liquid is DMF.

Under the assumption that water is perfectly conducting, simulation results were obtained for $0\le N_e\le 25$ by Notz & Basaran (1999). When $N_e=0$, gravitational dripping was dominant, and the pinchoff neck or the breakup location occurred at the bottom of the filament (or thread), which connects the pendant droplet to the nozzle. As N_e was increased, sufficient charges rapidly destabilized the liquid surface, and thereby reduced the pinchoff time (t or t_p), and the breakup location switched from the bottom of the filament to the top; see Fig. 3(a) at $N_e=11$. This switching behavior of the breakup location can be beneficial for improving the size uniformity of the droplet because the thread, which can possibly become a secondary or satellite droplet, can be easily merged into the primary pendant droplet. Also, when N_e was increased, the breakup length elongated during the gravitational dripping mode for $N_e<25$. At $N_e=25$, the typical microdripping mode of the EHD inkjet began to appear.

Our corresponding experimental results are shown in Fig. 3(b). Because of the perfect conductor assumption in the simulation, salt was maximally dissolved into the water up to the saturation point, at which the electrical conductivity of water was $K=54{,}100$ μS/cm. As N_e was increased up to $N_e=7.8$, the droplet size decreased, which did not agree with the simulation results, in which the droplet was maintained at almost the same size until $N_e=8$. The droplet shape or pinchoff topology was also different between the experiment and simulation. The droplet thinned and flattened at N_e lower than 7.8 in the experiment, while the droplet topology changed little in the simulation. For water with $K=54{,}100$ μS/cm, the typical microdripping mode of the EHD inkjet was shown at $N_e=7.8$, 8.3 and 9.7. To say exactly when microdripping begins is subjective. However, here we presumed that the microdripping mode begins when the droplet elongation is substantial enough to equal its width, a, of Fig. 1(b), which is equal or smaller than the nozzle diameter. At $N_e=9.7$, the droplet was the thinnest and smallest. Beyond $N_e=9.7$, the spray mode began, and the microdripping or drop-on-demand

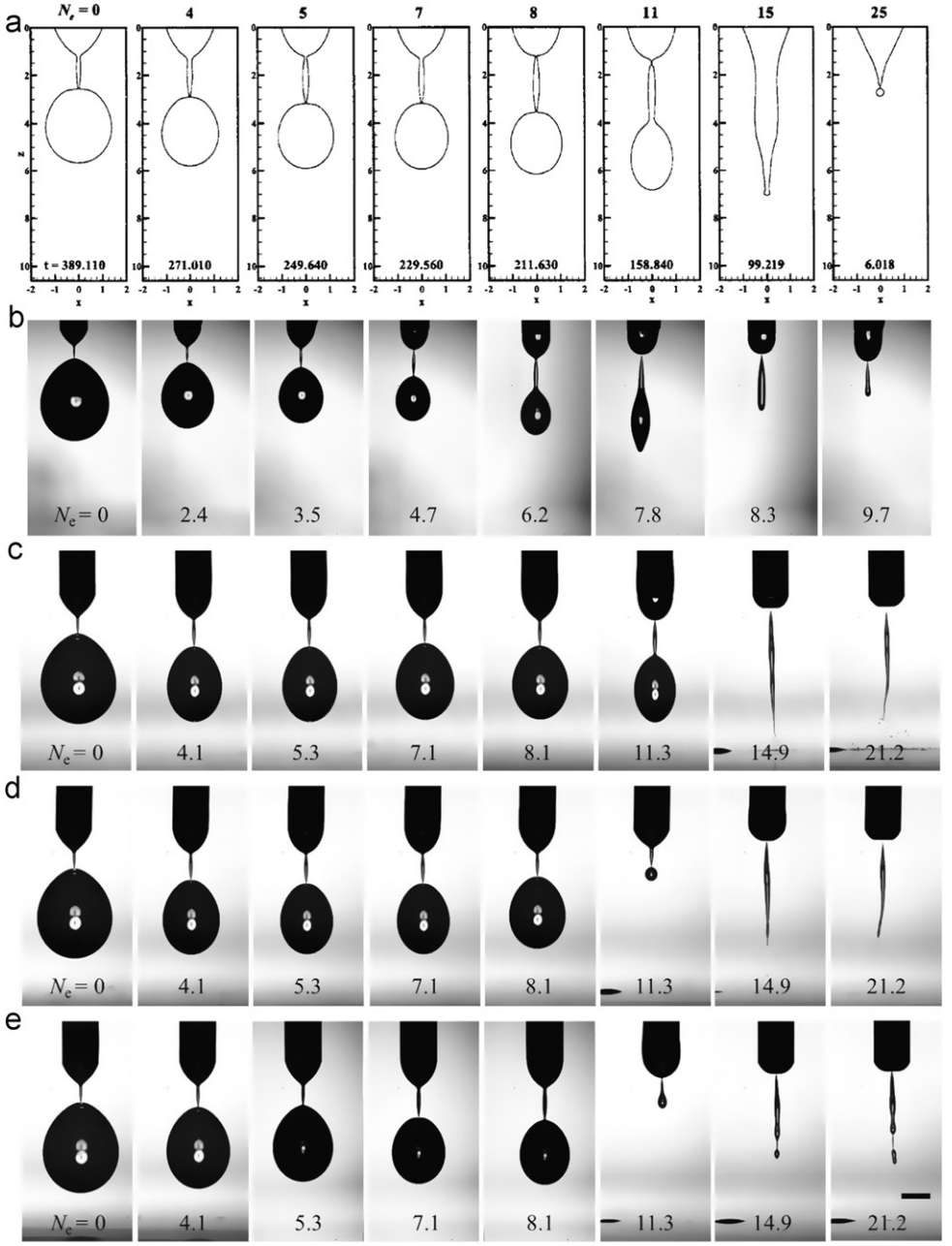

Fig. 3. Effect of dimensionless charging level, N_e, on the pinchoff behavior at various electrical conductivities, K, for water and DMF. (a) Simulation by Notz & Basaran (1999) for water, $K=\infty$, $Bo=0.35$; (b) water, $K=54{,}100$ μS/cm, $Bo=0.10$; (c) DMF, $K=1.2$ μS/cm, $Bo=0.12$; (d) DMF, $K=123$ μS/cm, $Bo=0.12$; (e) DMF, $K=530$ μS/cm, $Bo=0.12$, where $Bo=gR^2\rho/\sigma$ and R is the capillary radius. N_e is defined as $N_e=\varepsilon V^2/(2R\sigma)$ (scale bar=1 mm).

(DOD) mode was no longer viable. As a result, we may conclude that the stable microdripping range for high conductivity water is about $7.8 \le N_e \le 9.7$.

In Fig. 3(c)–(e), pinchoff snapshots of DMF are shown at various charging levels of $0 \le N_e \le 21.2$. The rows correspond to electrical conductivities of $K=1.2$, 123, and 530 μS/cm for (c), (d), and (e), respectively, which were attained by increasing the amount of HNO_3. Only a few droplets of HNO_3 were required to adjust the conductivity and it was confirmed, based on our measurement that the physical properties of the DMF were unchanged. The microdripping mode began at $N_e=11.6$, 11.3, and 11.0 for $K=1.2$, 123, and 530 μS/cm, respectively (not shown here, except for the $K=123$ μS/cm case), suggesting that the higher the K, the less the N_e required. Less voltage was required for higher K liquids because of the increased charge transport efficiency. In general, N_e values for DMF were higher than those for water because of DMF's lower surface tension; consider the definition of $N_e=\varepsilon V^2/(2R\sigma)$.

When charges are excessive (i.e., for $N_e > 11.3$), an oval-shaped droplet transforms into a cylindrical jet. Due to the excessive charge, the jet acquires helical instability that produces fine *drops* at the leading edge of the jet, essentially forming a spray, which yields poor printing quality unsuitable for high-resolution printing; see Fig. 1(b). However, it is interesting to observe that the jet becomes more stable as K increases; compare snapshots for $N_e > 11.3$. In Fig. 3(e), the jet undergoes a nonlinear breakup into a series of droplets. Although this could be problematic for high-resolution printing, at least the droplets are aligned and therefore, they print like a single droplet upon impact due to eventual coalescence.

Fig. 4 presents snapshots of pinchoffs for acetone, methanol, ethanol, water, DMF, and methoxyethanol (in columns), where the rows represent the increasing electrical conductivities of K_o (top row), 100 K_o (middle row), and 500 K_o (bottom row), with K_o being the liquid's original conductivity. Conductivities are increased by adding small amounts of HNO_3, which do not alter the fluid's physical properties. As noted in Fig. 3, there is a narrow range of N_e that yields microdripping, and Fig. 4(a) is snapshots of pinchoffs at the low-end of the stable charge level ($N_{e,\mathrm{low}}$, below which gravitational dripping occurs). For $N_{e,\mathrm{low}}$ (Fig. 4(a)), the effects of viscosity are manifest in bulged microdroplets (look from left to right for acetone, methanol, ethanol, and methoxyethanol as viscosity increases; see Table 1). Fig. 4(b) is snapshots at the high-end of the stable charge level ($N_{e,\mathrm{high}}$), above which droplets acquire helical instabilities and eventually form a spray. In Fig. 4(b), microdroplets tend to elongate with increasing K (down columns); compare snapshots of acetone, methanol, and ethanol. At the high-end voltage ($N_{e,\mathrm{high}}$), K seems to be the more dominant factor that determines the droplet topology. In general, K, in response to the supplied charges, influences the liquid relaxation time as well as the subsequent jet elongation and the eventual instability. Based on the comparison between Fig. 4(a) and (b), increasing N_e causes more charges to redistribute along the droplet surface and to repel, which leads to surface stretching and the eventual elongation of the droplet. One should observe that all of these elongated droplets are prone to emitting fine "*drops*" (much smaller than "droplet"; see Fig. 1(b)) at their bottom-tips, unless the liquid surface tension is strong enough to hold the droplet intact. In a phenomenological perspective, this charge emission is quite similar to the Rayleigh jet, which is formed when the charge level of a droplet exceeds the Rayleigh (1882) limit. A Rayleigh explosion occurs when the charge level exceeds the Rayleigh limit because of increased surface charge density via the evaporation process. The emission of fine *drops* at the bottom tip of an elongated droplet occurs when the electric field is concentrated at the tip. Because water and DMF have relatively high surface tensions, their bottom surfaces remain intact. Fig. 4 can be summarized as follows: (i) jet elongation is due to the increase in K, (ii) bulging of the droplet is due to viscosity under negligible influences of K and σ; and (iii) emission of fine *drops* at the bottom tip of the pinchoff droplet can be prevented if σ is sufficiently large.

Fig. 5 shows the time-series snapshots of droplet formation at (a) low-end, (b) mid-end, and (c) high-end voltages for DMF. The snapshots were taken every $\Delta t = 312\ \mu s$; seven snapshots comprise one 2-ms voltage pulse, though only six snapshots are shown in Fig. 5. At the low-end voltage in Fig. 5(a), the pinchoff droplet of the microdripping mode exhibits the typical pinchoff shape of gravitational dripping of Fig. 1(a), rather than that of Fig. 1(b). The filament does not merge with the primary droplet and, thus, a satellite droplet is formed. For the mid- and high-end voltage cases in Fig. 5(b) and

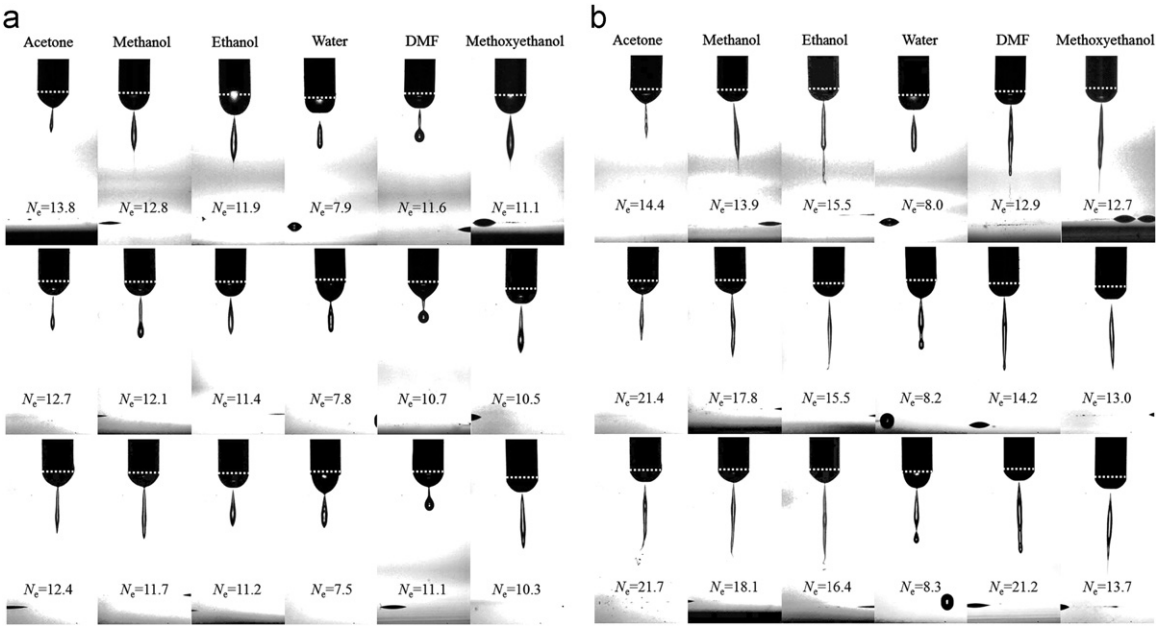

Fig. 4. Effect of K on the pinchoff droplets: (1st row) $K = K_o$, (2nd row) $K = 100\,K_o$, (3rd row) $K = 500\,K_o$, where K_o is the liquid's original electrical conductivity (scale bar = 1 mm). (a) *Low-end* voltage of stable microdripping N_e range. (b) *High-end* voltage of stable microdripping N_e range.

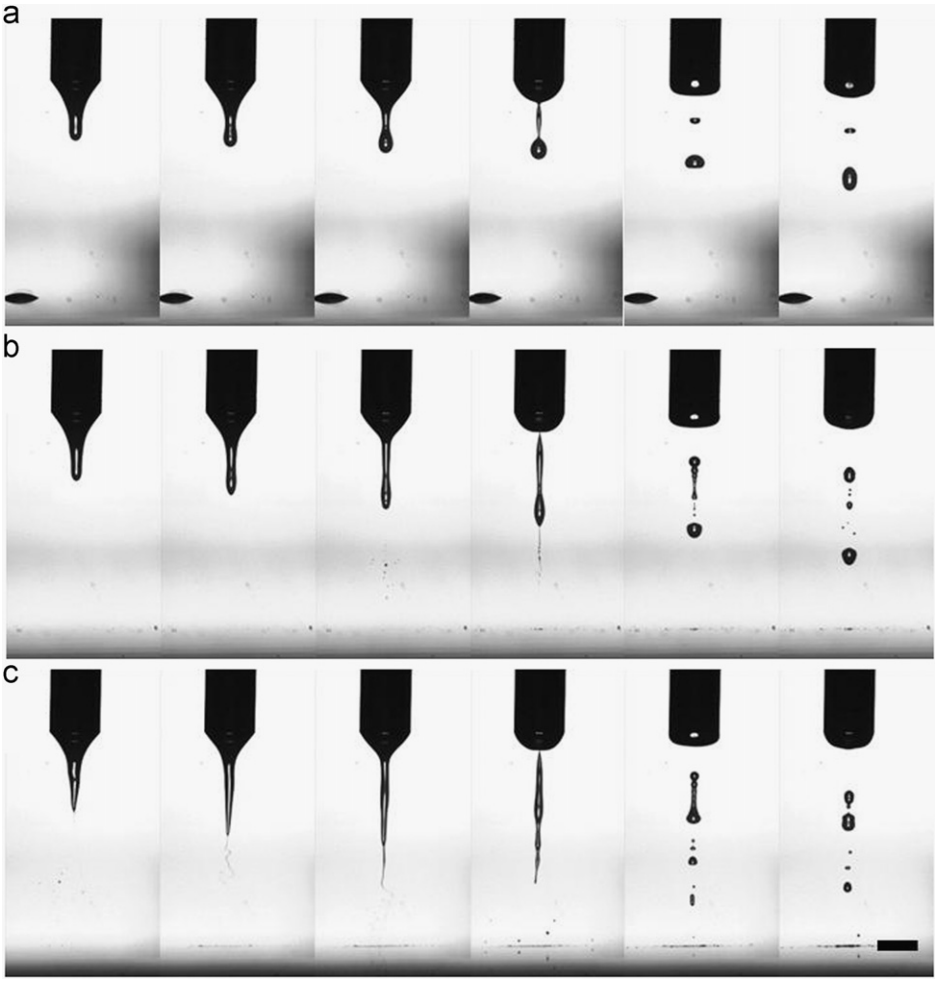

Fig. 5. Time-series snapshots for DMF at $K=K_o$, shown in Fig. 4. The time interval for the snapshots is $\Delta t=312$ μs. (a) Low-end voltage, $N_e=11.6$. (b) Mid-voltage, $N_e=12.1$. (c) High-end voltage, $N_e=12.9$ (scale bar=1 mm).

(c), respectively, multiple satellite droplets arise from nonlinear instabilities, typical of a (Rayleigh (1878) jet. Satellite droplets appear for all liquids, except for water, which has the highest surface tension. Thus, low-surface-tension fluids are prone to producing columnar jets that undergo Rayleigh instability.

Fig. 6(a) shows the aspect ratios of elongated microdrops as a function of N_e for various liquids at $K=K_o$. Aspect ratio is defined as the ratio of the vertical (b) to the horizontal (a) dimension of a droplet; AR$=b/a$ from Fig. 1(b). DMF has the smallest aspect ratio of AR≈ 3, while ethanol has the highest, AR≈ 17. For most liquids (except water), the microdripping regime is found in the range of $11.1 < N_e < 15.5$. For water, the N_e range for the microdripping regime is quite narrow (i.e., $7.9 < N_e < 8.0$) because of low $K_o=0.06$ μS/cm and high $\sigma=72$ mN/m. The N_e range for stable microdripping of water can be increased by adding salt or HNO_3. The N_e range for stable microdripping of water with increased conductivity of $K=54{,}100$ μS/cm as in Fig. 3(b) is found to be $7.2 < N_e < 9.7$. In general, because of a concentrated electric field, aspect ratio increases as N_e increases; this behavior is in agreement with the previous observation shown in Figs. 4 and 5. However, the rate of increase in AR differs from one another. The rates of AR change of methanol, DMF, and methoxyethanol are quite similar despite their substantial differences in K and μ.

Fig. 6(b) shows the vertical length of an elongated droplet or jet with respect to the nozzle diameter, whose range is $0.5 < b/d_n < 3$. All of the trends from Fig. 6(b) are similar to those shown in Fig. 6(a), except for some crossing points. It should be mentioned that, as N_e increases, the absolute vertical length (b) can reduce and the aspect ratio (b/a) increases. This is because the jet can become *significantly* thinner (a) but *moderately* shorter (b) as N_e increases. In other words, the rate of thinning (i.e., $|\Delta a/\Delta N_e|$) can be greater for an increased aspect ratio than that for a constant aspect ratio.

Fig. 7 quantitatively shows the effect of K on the aspect ratio for DMF. This effect is considered in conjunction with the qualitative data in Fig. 3(c)–(e). AR increases with K and N_e. However, the rate of increase in AR levels off at $N_e \approx 12$. In fact, for $N_e > 12.2$, the jet is actually shorter (albeit, notably thinner) because the leading-edge Rayleigh instabilities break up the front end of the jet.

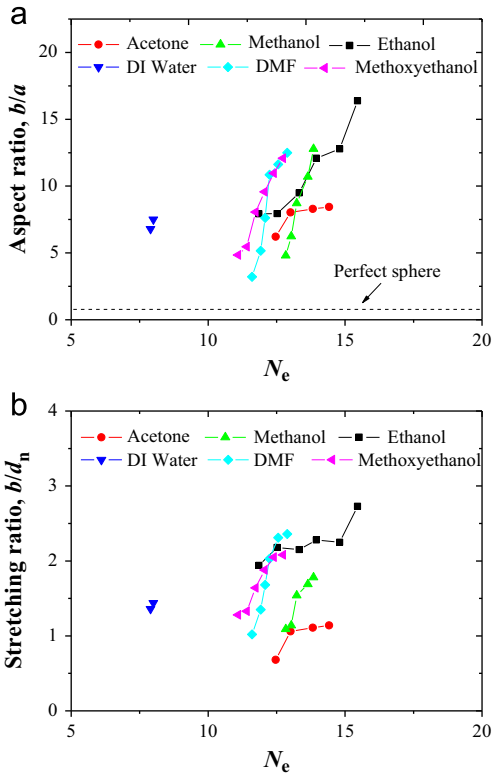

Fig. 6. Effect of N_e on the (a) aspect-ratio and (b) stretching-ratio of the pinchoff droplet for various liquids.

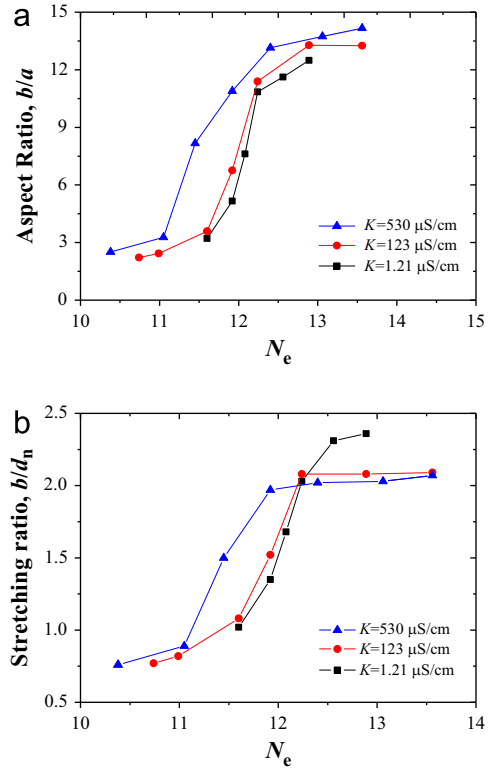

Fig. 7. Effect of electrical conductivity on the (a) aspect and (b) stretching ratio of the pinchoff droplet for DMF. K was varied by the addition of HNO_3.

To investigate the sole effect of K on pinchoff, N_e was fixed and K varied. In Fig. 8, the charging level is fixed at $N_e \approx 12.6$, and then the conductivity effect on the aspect ratio and that on the jet length were investigated. Despite the constant N_e, the pinchoff topology changed with different conductivities (K). The jet length is increased for greater K. This dependence of the jet length to K shows the significance effect of K on the pinchoff topology. Aspect ratio slightly decreased from acetone ($K=0.20$) to methanol ($K=0.31$), but increased again to ethanol ($K=0.70$) and to DMF ($K=1.21$). Fig. 8 confirms that the increase in K causes the elongation of the jet. Fig. 8 also implies that the dimensionless charging level, N_e, alone cannot characterize the topology of a charged pinchoff droplet because K plays an important role in shaping the topology of a pinchoff droplet. To reiterate the importance of K, we examined the topology of a pinchoff droplet under constant N_e and constant K for different liquids.

Fig. 9 shows the pinchoff behavior of a droplet for various liquids at constant N_e and K. As opposed to Fig. 8 where the difference in the jet length (b/d_n) and the aspect ratio (AR) among the liquids are due to varying K, a similar jet topology is shown in Fig. 9 because of the constant N_e and K, proving our claim that conductivity is an important parameter for characterizing pinchoffs behavior.

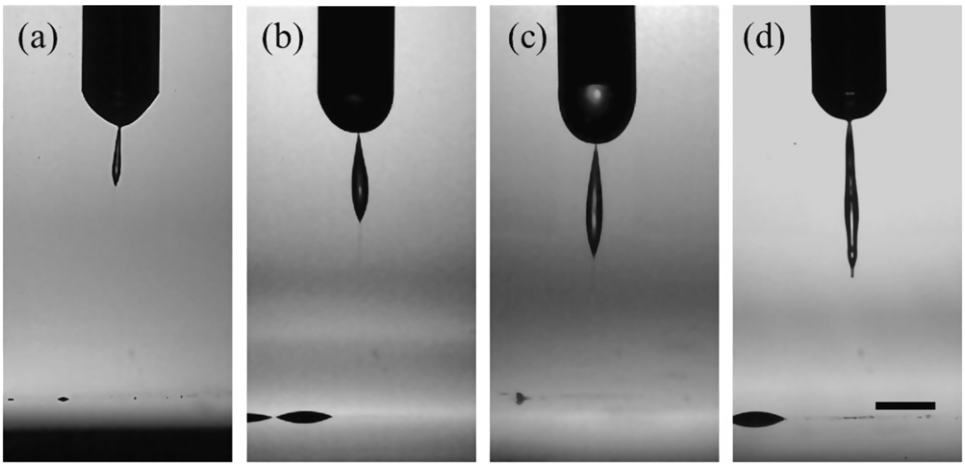

Fig. 8. Pinchoff behavior at constant voltage level ($N_e \approx 12.6$), but K differs by (a) $K=0.20$ μS/cm for acetone, (b) $K=0.31$ μS/cm for methanol, (c) $K=0.70$ μS/cm for ethanol, and (d) $K=1.21$ μS/cm for DMF. The aspect ratio changes from AR=6.22, 4.81, 7.94, and 11.62 for (a)–(d). The stretching ratio changes from $b/d_n=0.7$, 1.1, 2.2, and 2.4 for (a)–(d). The dimensionless charge relaxation time changes from $\alpha=\tau_e/\tau_\sigma=3.24$, 3.23, 1.02, and 1.03×10^{-3} s for (a)–(d).

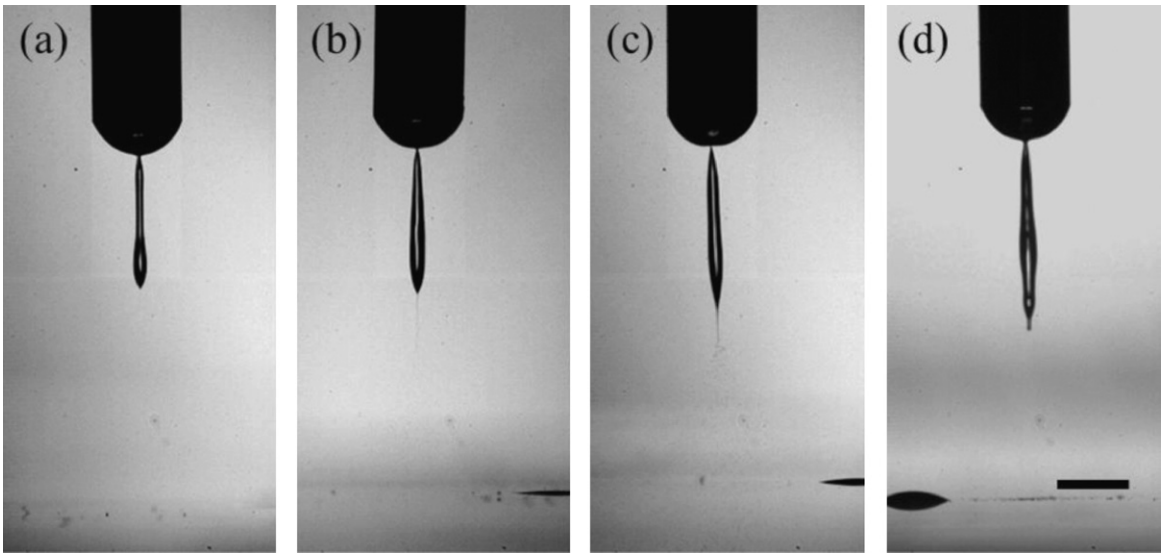

Fig. 9. Pinchoff behavior of various liquids at constant voltage level ($N_e \approx 12.6$), and $K=1.2$ μS/cm. The aspect ratio changes from AR=9.4, 10.43, 10.95, and 11.62 for (a)–(d). The stretching ratio changes from $b/d_n=1.48$, 1.61, 1.81, and 2.4 for (a)–(d). The dimensionless charge relaxation time changes from $\alpha=\tau_e/\tau_\sigma=0.54$, 0.82, 0.59, and 1.03×10^{-3} s for (a)–(d).

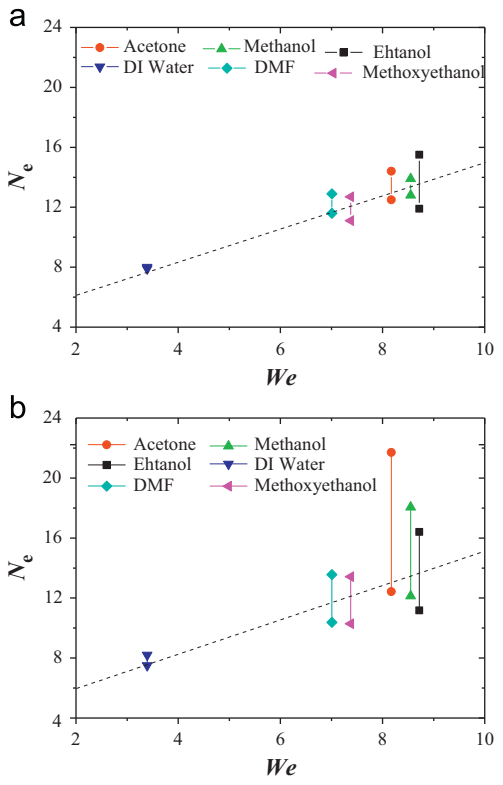

Fig. 10. The effect of K on the N_e range for the stable microdripping regime for various liquids. (a) $K=K_o$ and (b) $K=500\,K_o$.

Fig. 10 shows the effect of K on the stable N_e range for the stable microdripping regime. Increasing the conductivity from K_o to 500 K_o widens the stable microdripping N_e range (i.e., the range for N_e increases from (a) to (b)). A wider range of N_e for producing a stable microdripping droplet can be obtained by optionally adding HNO_3 or the like. Fig. 10 also shows that the charge level required to yield stable microdroplets increases with the Weber number (We), supporting the hypothesis that the surface tension force is one of the dominant factors controlling pinchoff behavior.

4. Conclusion

Effects of electrical conductivity, charge level, and surface tension on the pinchoff behavior of a droplet from an EHD inkjet were investigated. The range of the dimensionless charging level (N_e) that yielded stable microdripping droplets was reported for various liquids (i.e., acetone, methanol, ethanol, water, dimethylformamide, and methooxyethanol). We experimentally showed that the pinchoff topology was a function of both N_e and K for liquids with small relaxation time ($\alpha \ll 1$) and low viscosity ($Oh \ll \Theta(1)$). Despite the different properties of the liquids, the pinchoff topologies were similar when N_e and K were set constant.

Acknowledgment

This work was supported by the Human Resources Development of the Korea Institute of Energy Technology Evaluation and Planning (KETEP, No. 20104010100640), National Research Foundation of Korea (NRF-2012-0001169), and the Converging Research Center Program through the Ministry of Education, Science and Technology (2010K000969). This work was also supported by the National Research Foundation of Korea (NRF-2011-0030433 and 2010-0010217) grant funded by the Korean government (MEST) and a special grant for the KUCE Crimson Professorship by Korea University.

References

Basaran, O.A. (2002). Small-scale free surface flows with breakup: drop formation and emerging applications. *AIChE Journal*, *48*, 1842–1848.
Cheng, K., Yang, M.H., Chiu, W.W., Huang, C.Y., Chang, J., Ying, T.F., & Yang, Y. (2005). Ink-jet printing, self-assembled polyelectrolytes, and electroless plating: Low cost fabrication of circuits on a flexible substrate at room temperature. *Macromolecular Rapid Communications*, *26*, 247–264.
Choi, J.Y., Kim, Y.J., Lee, S., Son, S.U., Ko, H.S., Nguyen, V.D., & Byun, D.Y. (2008). Drop-on-demand printing of conductive ink by electrostatic field induced inkjet head. *Applied Physics Letters*, *93*, 193508–193510.

Collins, R.T., Harris, M.T., & Basaran, O.A. (2007). Breakup of electrified jets. *Journal of Fluid Mechanics*, *588*, 75–129.
Collins, R.T., Jones, J.J., Harris, M.T., & Basaran, O.A. (2008). Electrohydrodynamic tip streaming and emission of charged drops from liquid cones. *Nature Physics*, *4*, 149–154.
Eom, S.H., Senthilarasu, S., Uthirakumar, P., Hong, C.H., Lee, Y.S., Lim, J.S., Yoon, S.C., Lee, C.J., & Lee, S.H. (2008). Preparation and characterization of nano-scale ZnO as a buffer layer for inkjet printing of silver cathode in polymer solar cells. *Solar Energy Materials and Solar Cells*, *92*, 564–570.
Eom, S.H., Senthilarasu, S., Uthirakumar, P., Yoon, S.C., Lim, J.S., Lee, C.J., Lim, H.S., Lee, J., & Lee, S.H. (2009). Polymer solar cells based on inkjet-printed PEDOT:PSS layer. *Organic Electronics*, *10*, 536–542.
Gilbert, W. (1628). *On the Magnet and Magnetic Bodies, and on That Great Magnet the Earth*. Peter Short: London.
Harris, M.T., & Basaran, O.A. (1993). Capillary electrostatics of conducting drops hanging from a nozzle in an electric field. *Journal of Colloid and Interface Science*, *161*, 389–413.
Jang, D., Kim, D., & Moon, J. (2009). Influence of fluid physical properties on ink-jet printability. *Langmuir*, *25*, 2629–2635.
Jaworek, A., & Sobczyk, A.T. (2008). Electrospraying route to nanotechnology: An overview. *Journal of Electrostatics*, *66*, 197–219.
Jayasinghe, S.N., & Edirisinghe, M.J. (2002). Effect of viscosity on the size of relics produced by electrostatic atomization. *Journal of Aerosol Science*, *33*, 1379–1388.
Kang, D.K., Lee, M.W., Kim, H.Y., James, S.C., & Yoon, S.S. (2011). Electrohydrodynamic pulsed-inkjet characteristics of various inks containing aluminum particles. *Journal of Aerosol Science*, *42*, 621–630.
Lee, M.W., Kang, D.K., Kim, N.Y., Kim, H.Y., James, S.C., & Yoon, S.S. (2012). A study of ejection modes for pulsed-DC electrohydrodynamic inkjet printing. *Journal of Aerosol Science*, *46*, 1–6.
Lee, M.W., Kang, D.K., Yoon, S.S., & Yarin, A.L. (2012). Coalescence of two drops on partially wettable substrates. *Langmuir*, *28*, 3791–3798.
Lister, J.R., & Stone, H.A. (1998). Capillary breakup of a viscous thread surrounded by another viscous fluid. *Physics of Fluids*, *10*, 2758.
Miao, P., & Xiao, P. (2002). Formation of ceramic thin films using electrospray in cone-jet mode. *IEEE Transactions on Industry Applications*, *38*, 50–56.
Nguyen, V.D., Schrlau, M.G., Tran, S.B.Q., Bau, H.H., Ko, H.S., & Byun, D. (2009). Fabrication of nanoscale nozzle for electrohydrodynamic (EHD) inkjet head and high precision patterning by drop-on-demand operation. *Journal of Nanoscience and Nanotechnology*, *9*, 7298–7302.
Notz, P.K., & Basaran, O.A. (1999). Dynamics of drop formation in an electric field. *Journal of Colloid and Interface Science*, *213*, 218–237.
Rayleigh, L. (1878). On the instability of jets. *Proceedings of the London Mathematical Society*, *10*, 4–13.
Rayleigh, L. (1882). On the equilibrium of liquid conducting masses charged with electricity. *Philosophical Magazine*, *14*, 184–186.
Taylor, G. (1964). Disintegration of water drops in an electric field. *Proceeding of the Royal Society A*, 383–397.
Wang, K., Paine, M.D., & Stark, J.P.W. (2009a). Freeform fabrication of metallic patterns by unforced electrohydrodynamic jet printing of organic silver ink. *Journal of Material Science*, *20*, 1154–1157.
Wang, K., Paine, M.D., & Stark, J.P.W. (2009b). Fully voltage-controlled electrohydrodynamic jet printing of conductive silver tracks with a sub-100 μm linewidth. *Journal of Applied Physics*, *106*, 024907.
Wang, K., & Stark, J.P.W. (2010). Direct fabrication of electrically functional microstructures by fully voltage-controlled electrohydrodynamic jet printing of silver nano-ink. *Applied Physics A*, *99*, 763–766.
Wu, N., & Russel, W.B. (2009). Micro- and nano-patterns created via electrohydrodynamic Instabilities. *Nano Today*, *4*, 180–192.
Yarin, A.L., Koombhongse, S., & Reneker, D.H. (2001). Taylor cone and jetting from liquid droplets in electrospinning of nanofibers. *Journal of Applied Physics*, *90*, 4836–4846.
Yu, J.H., Kim, S.Y., & Hwang, J. (2007). Effect of viscosity of silver nanoparticle suspension on conductive line patterned by electrohydrodynamic jet printing. *Applied Physics A*, *89*, 157–159.
Yudistira, H.T., Nguyen, V.D., Dutta, P., & Byun, D. (2010). Flight behavior of charged droplets in electrohydrodynamic inkjet printing. *Applied Physics Letters*, *96*, 023503.
Zhang, X., & Basaran, O.A. (1996). Dynamics of drop formation from a capillary in the presence of an electric field. *Journal of Fluid Mechanics*, *326*, 239–263.